

Simultaneous guidance of electromagnetic and elastic waves via glide symmetry phoxonic crystal waveguides

Lin-Lin Lei(雷林霖), Ling-Juan He(何灵娟), Qing-Hua Liao(廖清华), Wen-Xing Liu(刘文兴), and Tian-Bao Yu(于天宝)

Citation: Chin. Phys. B, 2024, 33 (**3**): 034202. DOI: 10.1088/1674-1056/ad0ec7
Journal homepage: http://cpb.iphy.ac.cn; http://iopscience.iop.org/cpb

What follows is a list of articles you may be interested in

Singular optical propagation properties of two types of one-dimensional anti-$\mathcal{PT}$-symmetric periodic ring optical waveguide networks

Yanglong Fan(樊阳龙), Xiangbo Yang(杨湘波), Huada Lian(练华达), Runkai Chen(陈润楷), Pengbo Zhu(朱蓬勃), Dongmei Deng(邓冬梅), Hongzhan Liu(刘宏展), and Zhongchao Wei(韦中超)
Chin. Phys. B, 2024, 33 (**3**): 034201. DOI: 10.1088/1674-1056/ad12ab

Silicon-based optoelectronic heterogeneous integration for optical interconnection

Le-Liang Li(李乐良), Gui-Ke Li(李贵柯), Zhao Zhang(张钊), Jian Liu(刘剑), Nan-Jian Wu(吴南健), Kai-You Wang(王开友), Nan Qi(祁楠), and Li-Yuan Liu(刘力源)
Chin. Phys. B, 2024, 33 (**2**): 024201. DOI: 10.1088/1674-1056/ad0e5b

Nonlinear perturbation of a high-order exceptional point: Skin discrete breathers and the hierarchical power-law scaling

Hui Jiang(江慧), Enhong Cheng(成恩宏), Ziyu Zhou(周子榆), and Li-Jun Lang(郎利君)
Chin. Phys. B, 2023, 32 (**8**): 084203. DOI: 10.1088/1674-1056/accb47

High-performance chiral all-optical OR logic gate based on topological edge states of valley photonic crystal

Xiaorong Wang(王晓蓉), Hongming Fei(费宏明), Han Lin(林瀚), Min Wu(武敏), Lijuan Kang(康丽娟), Mingda Zhang(张明达), Xin Liu(刘欣), Yibiao Yang(杨毅彪), and Liantuan Xiao(肖连团)
Chin. Phys. B, 2023, 32 (**7**): 074205. DOI: 10.1088/1674-1056/accb41

Dynamic light storage based on controllable electromagnetically induced transparency effect

Liu-Ying Zeng(曾柳莹), Jun-Fang Wu(吴俊芳), and Chao Li(李潮)
Chin. Phys. B, 2023, 32 (**6**): 064213. DOI: 10.1088/1674-1056/acd2bd

---

Simultaneous guidance of electromagnetic and elastic waves via glide symmetry phoxonic crystal waveguides

Lin-Lin Lei(雷林霖), Ling-Juan He(何灵娟)†, Qing-Hua Liao(廖清华), Wen-Xing Liu(刘文兴), and Tian-Bao Yu(于天宝)

School of Physics and Materials Science, Nanchang University, Nanchang 330031, *China*

(Received 25 September 2023; revised manuscript received 20 November 2023; accepted manuscript online 22 November 2023)

A phoxonic crystal waveguide with the glide symmetry is designed, in which both electromagnetic and elastic waves can propagate along the glide plane at the same time. Due to the glide symmetry, the bands of the phoxonic crystal supercell degenerate in pairs at the boundary of the Brillouin zone. This is the so-called band-sticking effect and it causes the appearance of gapless guided-modes. By adjusting the magnitude of the glide dislocation the edge bandgaps, the bandgap of the guided-modes at the boundary of the Brillouin zone, can be further adjusted. The photonic and phononic guided-modes can then possess only one mode for a certain frequency with relatively low group velocities, achieving single-mode guided-bands with relatively flat dispersion relationship. In addition, there exists acousto–optic interaction in the cavity constructed by the glide plane. The proposed waveguide has potential applications in the design of novel optomechanical devices.

Keywords: phoxonic crystals, glide symmetry, waveguide, acousto–optic interaction

PACS: 42.25.Bs, 42.70.Qs, 42.79.Jq **DOI:** 10.1088/1674-1056/ad0ec7

1. Introduction

Phoxonic crystals (PXCs), in which permittivities and elastic properties are periodically arranged in the same lattice on a common wavelength scale, are designed to synchronously control the behavior of electromagnetic and elastic waves and to enhance the opto–acoustic interaction.[1–15] The most significant characteristic of PXCs is the simultaneous photonic and phononic bandgaps, or the phoxonic bandgaps, resulting from multiple scattering of photons and phonons, in which transmission of waves is forbidden.[16] The existence of phoxonic bandgaps provides an opportunity for designing phoxonic devices and functional materials.[17–20] Past researches have shown that by introducing a linear gapped defect into an otherwise perfect PXC, electromagnetic and elastic waves can travel along the defect at the same time when guided modes are excited, forming a PXC gapped waveguide.[21–23] The waveguide not only can guide the waves but also can enhance their interaction because of the simultaneous confinement of photons and phonons.[21,24,25] However, the waveguides depending on the gapped defects are usually multimodal, leading a competition of the guided bands inside the complete bandgap that can severely flatten the guided bands.[26] Thus, it is necessary to explore a new manner to achieve single-mode phoxonic guided modes.

Decades ago, structures with higher symmetries, including twist, glide, and their combination, have been utilized to design novel waveguides.[27] However, only recently has there been a resurgence of interest in these higher symmetries in order to manipulate electromagnetic and airborne acoustic waves. A periodic structure has a glide symmetry (GS) if it remains invariant after a translation and a mirroring with respect to a plane called the glide plane. The most salient characteristics the GS given are the band-sticking or degeneracy at the boundary of the first Brillouin zone (FBZ), which offers a new route to design the band dispersion and gives rise to distinctive applications in kinds of waveguides. For example, GS can be used to decrease the dispersion and to widen the bandwidth.[28] Furthermore, GS can be able to improve gain and bandwidth of leaky-wave and lens antennas, and can boost the performance of phase shifters and filters realized in standard and groove-gap waveguide technologies.[29–31] These properties were found in various periodic structures, confirming that the benefits of GS are applicable to a wide range of practical waveguide devices. These waveguides are usually one-dimensional (1D) periodic structures with only one unit cell perpendicular to the direction of the waveguide. The GS waveguides can also be extended to the two-dimensional (2D) periodic structures, like 2D photonic and phononic crystals.[2,32–36] For instance, GS combined with a linear gapped defect can be used to regulate the dispersion relationship of guided modes in a triangular photonic crystal.[37] GS waveguide without extra gapped linear defect has been realized in a square lattice phononic crystal to obtain gapless and GS-protected acoustic guided-modes.[26]

In this paper, we introduce the GS into PXCs, which enables simultaneous guidance of electromagnetic and elasitc waves along the glide plane. The GS provides an alternative way to to manipulate electromagnetic and elastic waves at the

†Corresponding author. E-mail: helingjuan_123@163.com

© 2024 Chinese Physical Society and IOP Publishing Ltd

same time. Moreover, the glide parameter that quantifies the magnitude of the dislocation can be used to adjust the size of the edge bandgaps, the bandgap of the guided-modes at the boundary of the Brillouin zone (BZ). This offers the waveguide a function of filtering electromagnetic and elasitc waves at the same time. Moreover, we find that the glide interface can also be used to construct a PXC cavity to enhance the acousto–optic (AO) interaction. Although the realization of the PXC waveguide is based on a square lattice, the principle can also be extended to other lattice types, like triangular lattices and honeycomb lattices.

2. Geometry and band structures of the PXC

The 2D PXC is made of silicon with air holes periodically arranged in a square lattice, as shown in Fig. 1(a). The lattice constant a is set to be 400 nm and the radius r of the air hole is $0.46a$. Introducing a glide dislocation with a non-zero glide parameter g along the glide plane $y = 0$, one half of the PXC is shifted by a certain distance in the x direction. The two sub-crystals are labeled in Fig. 1 as PXC1 and PXC2. Although the resultant PXC in Fig. 1(b) losses a translational symmetry in the y direction but gains the GS when $g = a/2$.[38–41] A glide symmetric structure overlaps with itself after a translation of $a/2$ and a reflection with respect to the glide plane. The material parameters of silicon are as follows: mass density $\rho = 2331$ kg/m^3, relative permittivity $\varepsilon = 12.5$, transverse and longitudinal sound speeds $v_t = 5360$ m/s and $v_l = 8950$ m/s, respectively.[20,42] The three independent stiffness coefficients of the silion material are: $C_{11} = 16.57 \times 10^{10}$ N·m^{-21}, $C_{12} = 6.39 \times 10^{10}$ N·m^{-21}, and $C_{44} = 7.962 \times 10^{10}$ N·m^{-21}.[43] Herein, the calculation of band structures and numerical simulations are based on the finite element methods.

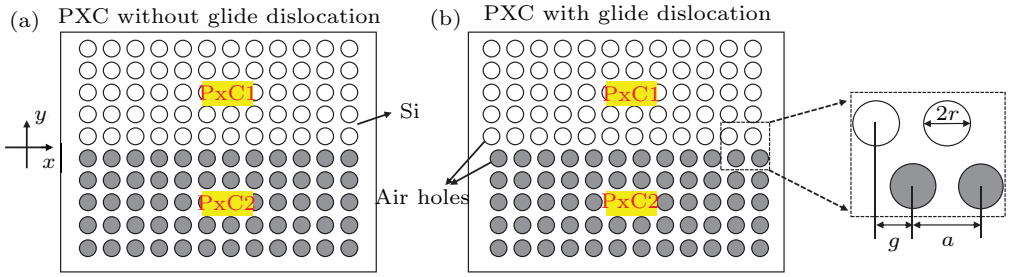


Fig. 1. Schematic diagram of the 2D PXC waveguide with air holes embedded into an Si host, spliced by two pieces of identical PXCs with air holes colored by white and grey, respectively. The two identical PXCs are labeled as PXC1 and PXC2. (a) PXC with glide parameter $g = 0$. (b) PXC with glide parameter $g = a/2$. The enlarged view in panel (b) shows the glide parameter g, lattice constant a, and diameter $2r$ of air holes.

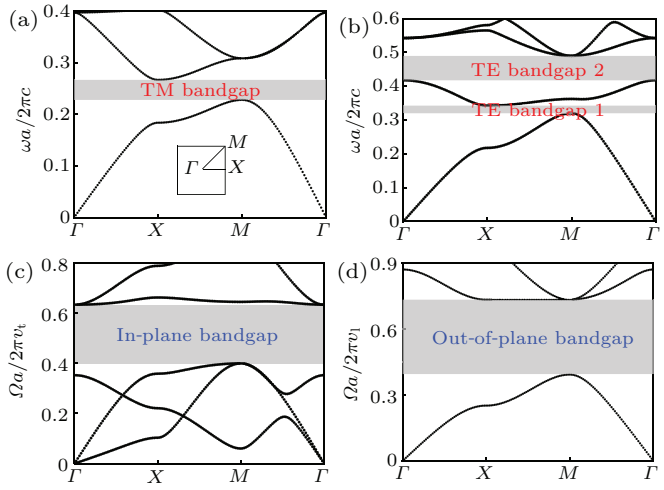


Fig. 2. Band structures of the PXC unit-cell. (a) Transverse magnetic (TM) modes having a complete bandgap between the first and second bands. (b) Transverse electric (TE) modes having two complete bandgaps, one between the first and second bands and the other between the second and third bands. (b) In-plane and (d) out-plane elastic modes, both of which show one complete bandgap.

We plot the phoxonic band structures for the unit-cell using Floquet periodic boundary conditions, as shown in Fig. 2. For photonic modes, we consider transverse magnetic (TM) modes with electric fields along the axis of the air holes and transverse electric (TE) modes with magnetic fields along the axis of the air holes. The TM and TE band structures are shown in Figs. 2(a) and 2(b), showing one and two complete bandgaps, respectivley. The inset in Fig. 2(a) is the FBZ, showing the highest symmetry points. For phononic modes, figures 2(c) and 2(d) show the band structures of in-plane and out-of-plane elastic modes, respectively, both of which possess one complete bandgap. We would like to clarify two points here. Although normalized center frequencies of photonic and phononic bandgaps are in the order of 10^{-1}, but the actual phononic frequency is typically orders of magnitude smaller than the photonic frequency for a common lattice constant a since the sound speed is much smaller than the light speed. Besides, their is no GS for the case in Fig. 1(a), and the unit-cell bands do not show the pairwise degenerate points at the X point of the FBZ.

3. Regulation of the glide dislocation on the phoxonic guided modes

To explore the existence of the phoxonic guided modes, we plot the band structures of the supercell composed of 10 unit-cells with $g = 0$, as shown in Fig. 3. In the calculation, periodic boundary conditions are applied to the x direc-

tion, while perfect-electric-conductor and free boundary conditions are applied to the y direction for the photonic and phononic modes, respectively.[26,44] Not surprisingly, there are no guided modes located in the photonic (Figs. 3(a) and 3(b)) and phononic (Figs. 3(c) and 3(d)) bandgaps due to the absence of linear gapped defects or the topological phase transition along the y direction between the PXC1 and PXC2. Note that the doubly degenerated bands located in the in-plane elastic bandgap are the surface waves that travel along the upper and lower boundaries of the PXC.[26]

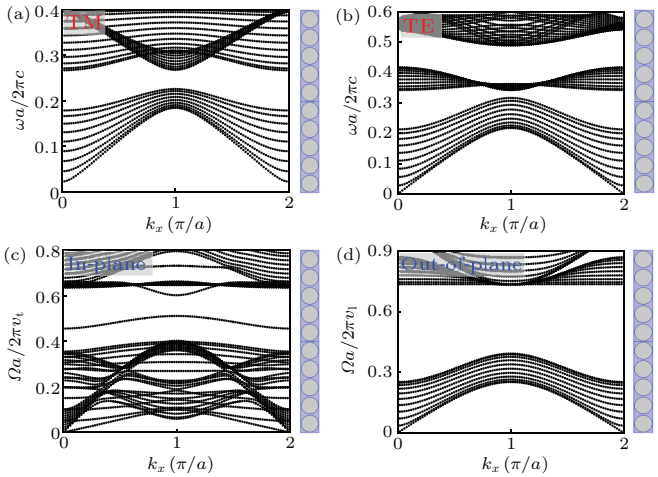


Fig. 3. Band structures of the PXC super-cell with $g = 0$ for (a) TM, (b) TE, (c) in-plane and (d) out-plane elastic modes. There are no guided modes lying in the super-cell bandgaps.

However, this situation will be changed when the GS is introduced into the PXC. The GS is achieved by a translation of the PXC2 with $g = a/2$. As a result, pairwise degenerate points would appear at the boundary of the BZ of the super-cell. To verify this, super-cell band structures for TM, TE, in-plane and out-of-plane elastic modes are plotted in Figs. 4(a)–4(d), respectively, from which we can see that all the bands are degenerate at the $k_x = \pi/a$. Moreover, there are two gapless modes located in the phoxonic bandgap, where there should be nothing. The right panels of Figs. 4(a), 4(c), and 4(d) show the fields of E_z, total displace u, and pressure P for TM, in-plane and out of plane in-gap modes for the higher-frequency branches at $k_x = 0.8\ (\pi/a)$, while the right panel of Fig. 4(b) shows the H_z field of TE in-gap modes at $k_x = 0.5\ (\pi/a)$, respectively. The positions of these modes are labelled by the green dots on the in-gap phoxonic modes. As can be seen, these phoxonic in-gapped modes are well confined at the interface between the PXC1 and PXC2, and the same thing is true for the lower-frequency branches of the in-gap modes. Therefore, they are interface modes not the surface modes that travel along the upper and lower boundaries of the PXC. Moreover, the photonic and phononic guided modes are single-mode within a relatively large frequency range. As the yellow shaded areas shown in Fig. 4, the frequency ranges of the single-modes are $0.21954\ (2\pi c/a) \sim 0.26590\ (2\pi c/a)$, $0.47274\ (2\pi c/a) \sim 0.49228\ (2\pi c/a)$, $0.43890\ (2\pi v_t/a) \sim 0.60028\ (2\pi v_t/a)$, and $0.38695\ (2\pi v_l/a) \sim 0.66134\ (2\pi v_l/a)$ for TM, TE, in-plane, and out-of-plane elastic modes, respectively.

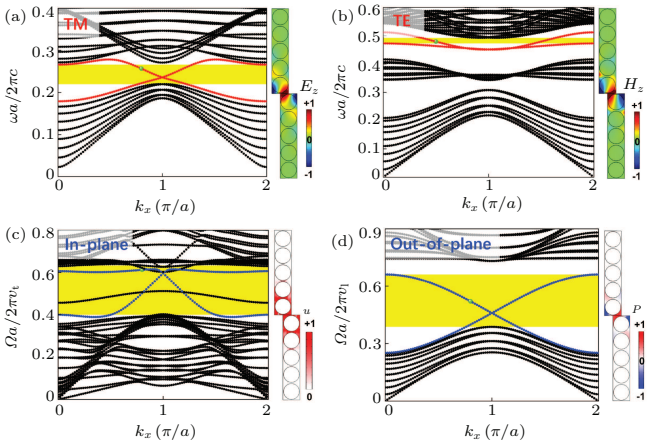


Fig. 4. Band structures of the PXC super-cell with $g = a/2$ for (a) TM, (b) TE, (c) in-plane, and (d) out-plane elastic modes. All the bands have to pairwise degenerate at $k_x = \pi/a$, the boundary of the FBZ of the super-cell, and there are two gapless guided modes located in the super-cell bandgaps. The green dot in each panel is one of the eigenmodes of the guided bands, and its eigenfield is shown in the right of the panel.

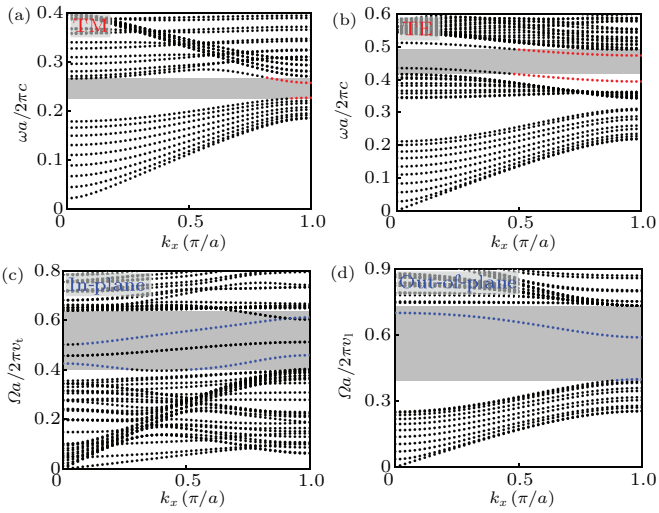


Fig. 5. Band structures of the PXC super-cell with $g = a/4$ for (a) TM, (b) TE, (c) in-plane, and (d) out-plane elastic modes. Band degeneracies vanish, and edge bandgaps appear at the boundary of the FBZ of the super-cell. The shaded areas denote the bandgaps.

If the glide parameter g deviates $a/2$, the gapless in-gap modes will be changed into gapped modes due to the broken of the GS. Figure 5 shows the super-cell bands for the case of $g = a/4$, and the shaded areas denote the bandgaps. As can be seen, all the band degeneracies vanish and the edge bandgap appears, and the guided-modes can thus possess only one mode for a certain frequency in the bandgap with relatively low group velocities. As a result, there are single-mode photonic and phononic guided modes located in their respective bandgaps, with relatively flat dispersion relationship. In particular, the group velocities of the in-gap modes approach to zero near the center and the boundary of BZ. This

would help to enhance the interaction between the electromagnetic waves and elastic waves due to the prolonged interaction time.[45] It is worth noting that the gapless guided-modes could only exit for $g = a/2$. Figure 6 gives a visualized process of the phoxonic guided-mode degeneracies. As g goes from 0 to $a/2$, the phoxonic edge bandgaps gradually close to zero at $a/2$. Thus, glide dislocation provides a degree of freedom to manipulate the phoxonic dispersion relationship and the size of edge bandgaps.

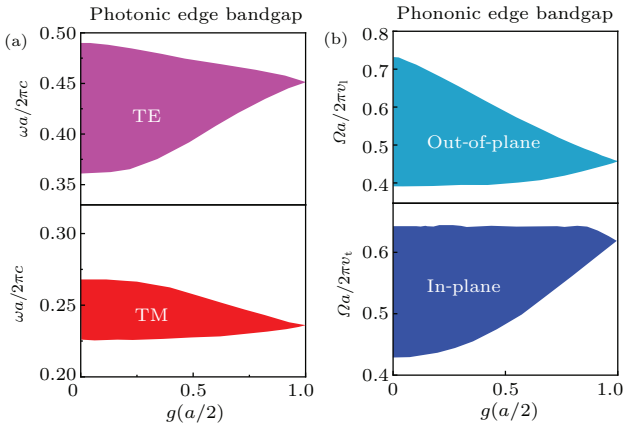


Fig. 6. Evolution processes of (a) photonic and (b) phononic edge bandgaps. Red and pink areas denote the bandgaps of TM and TE modes, while blue and cyan areas denote that of the in-plane and out-of-plane elastic modes, respectively. As g goes from 0 to $a/2$, the phoxonic edge bandgaps gradually close to zero.

Of note, not all the bulk bandgaps have the in-gap modes. In Fig. 4(b), the in-gap TE modes only exit in the second super-cell bandgap. In order to provide an explanation for the band degeneracy and why there are in-gap gapless modes, we introduce the glide symmetry operator $\hat{G}$, which is defined as $\hat{G}\psi(x,y) = \psi(x+a/2,-y)$, where ψ is the Bloch wave function. The combination of the glide symmetry operator $\hat{G}$ and time-reversal operator $\hat{\theta}$ gives $\hat{\Theta} = \hat{G}\hat{\theta}$. When acting on the ψ twice, $\hat{\Theta}^2\psi = \mathrm{e}^{\mathrm{i}k_x a}\psi$. Thus, $\hat{\Theta}^2\psi = -\psi$ at $k_x = \pi/a$, which forms the Kramers-like degeneracy and makes all bands to group in pairs at the $k_x = \pi/a$ including the nearest two bands on either side of the phoxonic band gaps.[46] Thus, if there is an odd number of bands below the super-cell bandgap, two in-gap gapless modes could exist; if there is an even number of bands below the super-cell bandgap, no in-gap gapless modes could exist since there is no extra band to degenerate with the bands above the bandgap. There are ten bands below the first TE super-cell bandgap, and thus no in-gap modes could exist there.

4. PXC waveguide with GS

As the phoxonic in-gap modes can be confined at the glide plane with nonvanishing group velocities, waves hence can travel along the glide plane when operating frequencies lie in the frequency range of in-gap modes. To verify this, a waveguide made of the PXC with GS is constructed, and figures 7(a)–7(d) show field distributions of E_z, H_z, in-plane and out-of-plane elastic modes when electromagnetic and elastic waves are incident from the left. The frequencies of the waves for TM, TE, in-plane, and out-of-plane modes are 0.25733 (c/a), 0.48000 (c/a), 0.56716 (v_t/a), and 0.52737 (v_l/a), respectively. As can be seen, the waves only travel along the glide plane with little energy permeated into the bulk PXC. Thus, these phoxonic in-gap modes are confined guided-modes.

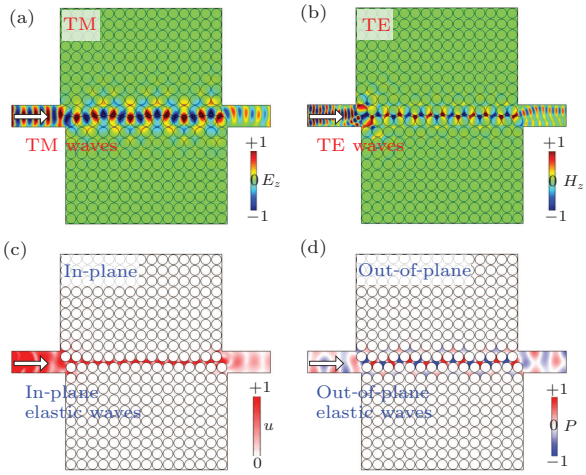


Fig. 7. Field distributions of the phoxonic waveguide with GS for (a) TM, (b) TE, (c) in-plane, and (d) out-of-plane modes with normalized frequencies 0.25733 (c/a), 0.48000 (c/a), 0.56716 (v_t/a), and 0.52737 (v_l/a), respectively, from which we can see that electromagnetic and elastic waves can only travel along the glide plane. The waves are incident from the left, indicated by the white arrows.

We further plot the transmittance for waveguides with and without GS in Fig. 8, indicated by the red solid lines and black dot-and-dash lines, respectively. For the PXC with GS, due to the existance of the gapless guided-modes, both the photonic (Figs. 8(a) and 8(b)) and phononic (Figs. 8(c) and 8(d)) modes show continuous and high transmittance within the super-cell bandgaps (indicated by the dashed areas). The blue dashed-lines in Fig. 8 show the phoxonic transmittance for $g = a/4$. Compared with the transmittance for $g = a/2$, extra transmittance dips appear for the TM, in-plane, and out-of-plane modes, while the transmittance dip moves towards the high-frequency range for TE modes. This is because when $g = a/4$ the phoxonic edge bandgaps are open, and the waves that used to pass through the GS waveguide cannot now. For the PXC with $g = 0$, no wave can enter the waveguide, since no guided modes exist in the bandgaps, as the black dot–dashed lines shown in Fig. 8. Thus, the glide parameter g offers a controllable variable to adjust the in-gap modes to change from gapless to gapped guided-modes for both the photonic and phononic modes, which contributes to select desired waveguide frequencies and to eliminate unwanted ones.

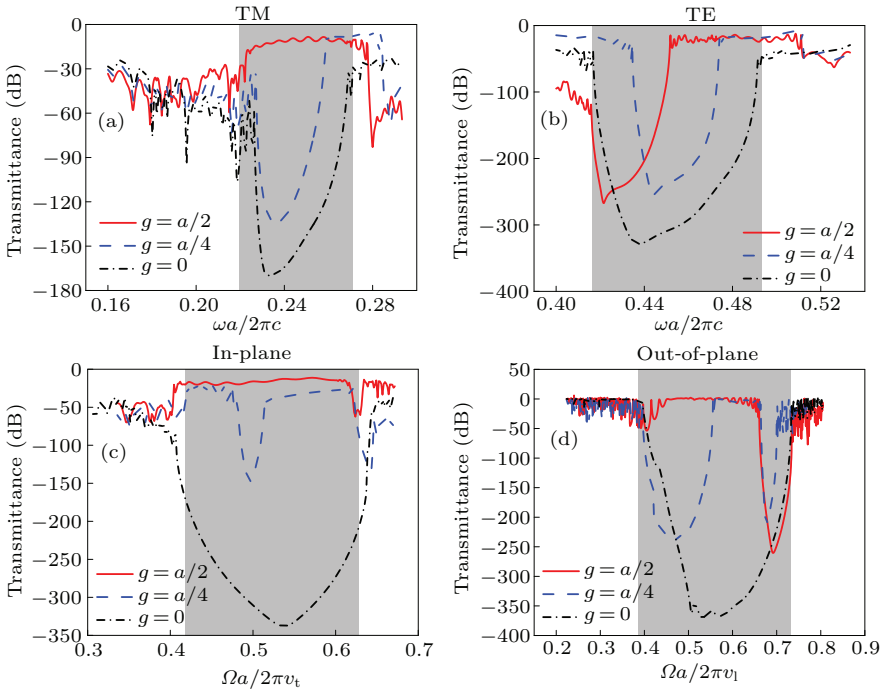


Fig. 8. Transmittance of (a) TM, (b) TE, (c) in-plane, and (d) out-of-plane elastic modes. Red solid lines, blue dashed lines, and black dash-and-dot lines denote transmittance of the waveguide for $g = a/2$, $g = a/4$, and $g = 0$, respectively. Shaded areas denote super-cell bandgaps.

5. Acousto–optic (AO) interaction

When photons and phonons are confined in a PXC cavity simultaneously, there would be enhanced AO interaction. Generally, the cavity is constructed by a point defect or a linear gapped defect. Here, we use the glide interface to construct a PXC cavity, and numerically demonstrate the cavity could confine the photons and phonons at the same time as well. As can be seen in Fig. 9, the electromagnetic waves and in-plane elastic waves can be well confined into the upper and lower boundaries of the inner boundary at the same time, and their normalized eigenfrequencies are 0.25908 (c/a), 0.48604 (c/a), and 0.60263 (v_t/a), respectively. The photonic and phononic eigenfield distribution are symmetric about the y axis. In the simulation, periodic boundary conditions are applied to the external boundaries of the PXC cavity. The simultaneous confinement would enhance the AO interaction, which can be quantified by optomechanical coupling rate, the frequency shift imparted by the zero-point motion of the mechanical resonator, where moving interfaces (MIs) and photoelastic (PE) effects are considered. The MI effect is due to the dynamic motion of the silicon–air interfaces, while the PE effect is related to the change of the refractive index by the generation of the strain field in the structure.[43] The full optomechanical coupling rate is $g_{\mathrm{OM}} = g_{\mathrm{OM,MI}} + g_{\mathrm{OM,PE}}$. Considering first-order perturbation theory, the PE contribution by unit thickness of the PXC is[47]

$$g_{\mathrm{OM,PE}} = -\frac{\omega_0}{2}\frac{\left\langle E\left|\frac{\partial\varepsilon}{\partial\alpha}\right|E\right\rangle}{\int \boldsymbol{E}^*\cdot D\mathrm{d}S}, \tag{1}$$

where

$$\left\langle E\left|\frac{\partial\varepsilon}{\partial\alpha}\right|E\right\rangle = -\varepsilon_0 n^4\int |E_2|^2(p_{12}S_{xx}+p_{12}S_{yy})\mathrm{d}S, \tag{2}$$

for the TM modes, and

$$\begin{aligned}\left\langle E\left|\frac{\partial\varepsilon}{\partial\alpha}\right|E\right\rangle = -\varepsilon_0 n^4\int \big[&2\mathrm{Re}\,E_x^*E_y p_{44}S_{xy}\\ &+|E_x|^2(p_{11}S_{xx}+p_{12}S_{yy})\\ &+|E_y|^2(p_{11}S_{yy}+p_{12}S_{xx})\big]\mathrm{d}S\end{aligned} \tag{3}$$

for the TE modes. S_{ij} $(i,j = x,y)$ is the elastic strain tensor.

The MI contribution by unit thickness of the PXC is given by

$$g_{\mathrm{OM,MI}} = -\frac{\omega_0}{2}\frac{\int(\boldsymbol{U}\cdot\boldsymbol{n})(\Delta\varepsilon\cdot\boldsymbol{E}_{\parallel}^2-\Delta\varepsilon^{-1}\cdot\boldsymbol{D}_{\perp}^2)\mathrm{d}l)}{\int \boldsymbol{E}^*\cdot D\mathrm{d}S}, \tag{4}$$

where $\boldsymbol{U}$ is the normalized displacement field, $\boldsymbol{n}$ is the outward facing surface normal, $\boldsymbol{E}$ is the electric field, $\boldsymbol{D}$ is the displacement field. The subscripts $\parallel$ and $\perp$ indicate respectively the component parallel and perpendicular to the surface of the electromagnetic field. The PE coefficients of silicon are: $p_{11} = -0.1$, $p_{12} = 0.01$, and $p_{44} = -0.05$. $\Delta\varepsilon = \varepsilon_{\mathrm{material}} - \varepsilon_{\mathrm{air}}$ and $\Delta\varepsilon^{-1} \equiv \varepsilon_{\mathrm{material}}^{-1} - \varepsilon_{\mathrm{air}}^{-1}$, where ε is the material permittivity. The integration is performed along the interfaces between the circular contour line of the hole and the Si matrix boundaries. The calculated optomechanical coupling rates per 1-nm thickness of the PXC for TM and TE modes are $g_{\mathrm{OM}} = g_{\mathrm{OM,MI}} + g_{\mathrm{OM,PE}} = -2.2\times10^{-5}\ (c/a) - 1\times10^{-6}\ (c/a) = -2.3\times10^{-5}\ (c/a)$ and $g_{\mathrm{OM}} = g_{\mathrm{OM,MI}} + g_{\mathrm{OM,PE}} = 1.5\times10^{-5}\ (c/a) - 3\times10^{-6}\ (c/a) = 1.2\times10^{-5}\ (c/a)$, respectively. The nonzero coupling rates show there exists interaction between photons and phonons, which would provide potential application in optomechanical devices.

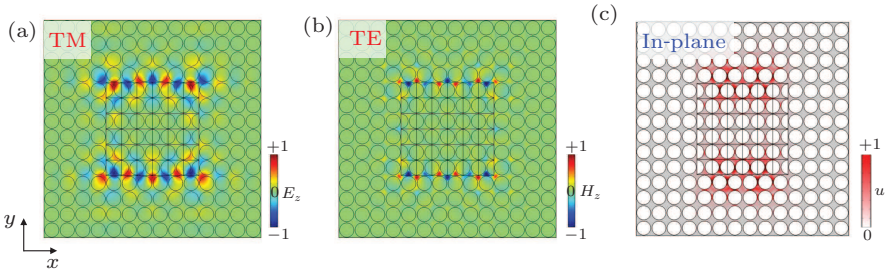


Fig. 9. Eigenfields of the cavity modes for TM, TE, and in-plane elastic modes, and their normalized frequencies are 0.25908 (c/a), 0.48604 (c/a), and 0.60263 (v_t/a), respectively.

6. Conclusion

In summary, a PXC waveguide with GS is proposed. Due to the band-sticking effect, a pair of gapless guided-modes appear in the phoxonic bandgaps. Furthermore, by changing the magnitude of the glide dislocation, the edge bandgaps and the dispersion relationship of the guided modes can be further adjusted, which helps to simultaneously achieve photonic and phononic single-mode guided bands with relatively flat dispersion relationship. By constructing a PXC cavity, there exists AO interaction due to the simultaneous confinement of electromagnetic waves and in-plane elastic waves. Our work has potential applications in the design of optomechanical devices, and the principle of realization can also be extended to other lattice types, like triangular lattices and honeycomb lattices.

Acknowledgements

Project supported by the National Natural Science Foundation of China (Grant No. 12064025), the Natural Science Foundation of Jiangxi Province, China (Grant No. 20212ACB202006), the Major Discipline Academic and Technical Leaders Training Program of Jiangxi Province, China (Grant No. 20204BCJ22012), and the Open Project of the Key Laboratory of Radar Imaging and Microwave Photonic Technology of the Education Ministry of China.

References

[1] Maldovan M and Thomas E 2006 *Appl. Phys. B* **83** 595
[2] Maldovan M and Thomas E L 2006 *Appl. Phys. Lett.* **88** 251907
[3] Eichenfield M, Camacho R, Chan J, Vahala K J and Painter O 2009 *Nature* **459** 550
[4] Favero I and Karrai K 2009 *Nat. Photon.* **3** 201
[5] Rolland Q, Oudich M, El-Jallal S, Dupont S, Pennec Y, Gazalet J, Kastelik J C, Lévêque G and Djafari-Rouhani B 2012 *Appl. Phys. Lett.* **101** 061109
[6] Lucklum R, Zubtsov M and Oseev A 2013 *Analytical and Bioanalytical Chemistry* **405** 6497
[7] Rolland Q, Dupont S, Gazalet J, Kastelik J C, Pennec Y, Djafari-Rouhani B and Laude V 2014 *Opt. Express* **22** 16288
[8] Escalante J M, Martínez A and Laude V 2014 *J. Appl. Phys.* **115** 064302
[9] Pennec Y, Rouhani B D, Boudouti E H E, Li C, Hassouani Y E, Vasseur J O, Papanikolaou N, Benchabane S, Laude V and Martinez A 2010 *Opt. Express* **18** 14301
[10] Mohammadi S, Eftekhar A A, Khelif A and Adibi A 2010 *Opt. Express* **18** 9164
[11] Kipfstuhl L, Guldner F, Riedrich-Möller J and Becher C 2014 *Opt. Express* **22** 12410
[12] Ma T X, Wang Y S and Zhang C 2017 *Crystals* **7** 350
[13] Moradi P and Bahrami A 2018 *J. Appl. Phys.* **123** 115113
[14] Qiu L, Shomroni I, Seidler P and Kippenberg T J 2020 *Phys. Rev. Lett.* **124** 173601
[15] Jin J, Wang X, Zhan L and Hu H 2021 *Nanotechnol. Rev.* **10** 443
[16] Aram M H and Khorasani S 2018 *J. Opt. Soc. Am. B* **35** 1390
[17] Xia B, Fan H and Liu T 2019 *Int. J. Mech. Sci.* **155** 197
[18] Aboutalebi S Z and Bahrami A 2021 *Phys. Scr.* **96** 075704
[19] Ma T X, Liu J, Zhang C and Wang Y S 2022 *Phys. Rev. A* **106** 043504
[20] Lei L L, He L J, Liu W X, Liao Q H and Yu T B 2022 *Appl. Phys. Lett.* **121** 193103
[21] Lin T R, Lin C H and Hsu J C 2013 *J. Appl. Phys.* **113** 053508
[22] Chiu C C, Chen W M, Sung K W and Hsiao F L 2017 *Opt. Express* **25** 6076
[23] Ma T X, Wang Y S, Zhang C and Su X X 2014 *J. Opt.* **16** 085002
[24] Laude V, Beugnot J C, Benchabane S, Pennec Y, Djafari-Rouhani B, Papanikolaou N, Escalante J M and Martinez A 2011 *Opt. Express* **19** 9690
[25] Shu Y, Yu M, Yu T, Liu W, Wang T and Liao Q 2020 *Opt. Express* **28** 24813
[26] Martínez J A I, Laforge N, Kadic M and Laude V 2022 *Phys. Rev. B* **106** 064304
[27] Tuevedo-Teruel O, Chen Q, Mesa F, Fonseca N J G and Valerio G 2021 *IEEE J. Microwaves* **1** 457
[28] Dahlberg O, Mitchell-Thomas R C and Quevedo-Teruel O 2017 *Sci. Rep.* **7**
[29] Beadle J G, Hooper I R, Sambles J R and Hibbins A P 2019 *J. Acoust. Soc. Am.* **145** 3190
[30] Janković N and Alù A 2021 *Phys. Rev. Appl.* **15** 024004
[31] Abdollahy H, Farahbakhsh A and Ostovarzadeh M H 2021 *AEU - International Journal of Electronics and Communications* **132** 153655
[32] Mahmoodian S, Prindal-Nielsen K, Söllner I, Stobbe S and Lodahl P 2016 *Opt. Mater. Express* **7** 43
[33] Yoshimi H, Yamaguchi T, Ota Y, Arakawa Y and Iwamoto S 2020 *Opt. Lett.* **45** 2648
[34] Yoshimi H, Yamaguchi T, Katsumi R, Ota Y, Arakawa Y and Iwamoto S 2021 *Opt. Express* **29** 13441
[35] Xie X, Yan S, Dang J, Yang J, Xiao S, Wang Y, Shi S, Yang L, Dai D, Yuan Y, Luo N, Cui T, Chi G, Zuo Z, Li B B, Wang C and Xu X 2021 *Phys. Rev. Appl.* **16** 014036
[36] Wen E, Bisharat D J, Davis R J, Yang X and Sievenpiper D F 2022 *Phys. Rev. Appl.* **17** 064008
[37] Mock A, Lu L and O'Brien J 2010 *Phys. Rev. B* **81** 155115
[38] Kim H and Murakami S 2020 *Phys. Rev. B* **102** 195202
[39] Ghasemifard F, Norgren M and Quevedo-Teruel O 2018 *Sci. Rep.* **8** 11266
[40] Zhang S L and Zhou Q 2017 *Phys. Rev. A* **95** 061601
[41] Nica E M, Yu R and Si Q 2015 *Phys. Rev. B* **92** 174520
[42] Lei L, Yu T, Liu W, Wang T and Liao Q 2021 *Opt. Express* **30** 308
[43] Shu Y, Yu M, Yu T, Liu W, Wang T and Liao Q 2020 *Opt. Express* **28** 24813
[44] Lei L, Xiao S, Liu W, Liao Q, He L and Yu T 2023 *Phys. Rev. Appl.* **20** 024014
[45] Yu Z and Sun X 2018 *Opt. Express* **26** 1255
[46] Lin Z K, Wang H X, Xiong Z, Lu M H and Jiang J H 2020 *Phys. Rev. B* **102** 035105
[47] El-jallal S, Oudich M, Pennec Y, Djafari-Rouhani B, Makhoute A, Rolland Q, Dupont S and Gazalet J 2013 *J. Phys.: Condens. Matter* **26** 015005